




# UniLiDAR: Bridge the domain gap among different LiDARs for continual learning

Zikun Xu<sup>1</sup>, Jianqiang Wang<sup>1,†</sup>, and Shaobing Xu<sup>1,†</sup>

School of Vehicle and Mobility, Tsinghua University, Beijing 100084, China

**Abstract.** LiDAR-based 3D perception algorithms have evolved rapidly alongside the emergence of large datasets. Nonetheless, considerable performance degradation often ensues when models trained on a specific dataset are applied to other datasets or real-world scenarios with different LiDAR. This paper aims to develop a unified model capable of handling different LiDARs, enabling continual learning across diverse LiDAR datasets and seamless deployment across heterogeneous platforms. We observe that the gaps among datasets primarily manifest in geometric disparities (such as variations in beams and point counts) and semantic inconsistencies (taxonomy conflicts). To this end, this paper proposes UniLiDAR, an occupancy prediction pipeline that leverages geometric realignment and semantic label mapping to facilitate multiple datasets training and mitigate performance degradation during deployment on heterogeneous platforms. Moreover, our method can be easily combined with existing 3D perception models. The efficacy of the proposed approach in bridging LiDAR domain gaps is verified by comprehensive experiments on two prominent datasets: OpenOccupancy-nuScenes and SemanticKITTI. UniLiDAR elevates the mIoU of occupancy prediction by **15.7%** and **12.5%**, respectively, compared to the model trained on the directly merged dataset. Moreover, it outperforms several SOTA methods trained on individual datasets. We expect our research to facilitate further study of 3D generalization, the code will be available soon.

**Keywords:** 3D occupancy prediction · Model generalization · Multiple datasets continual learning

## 1 Introduction

With the capability to acquire precise geometric information of entire scenes, LiDAR has become an indispensable sensor for most autonomous cars. LiDAR-based models play an important role in various crucial perception tasks for autonomous vehicles, including 3D object detection [10, 19, 23], semantic segmentation [13, 17, 33], and scene completion [9, 26, 28].

Current LiDAR-based models adhere to the paradigm of training and testing within a single dataset, thus constraining the source data to a limited domain. However, deploying dataset-specific models directly onto other datasets or

<sup>1</sup> †Corresponding author: shaobxu@tsinghua.edu.cn, wjqlws@tsinghua.edu.cn.

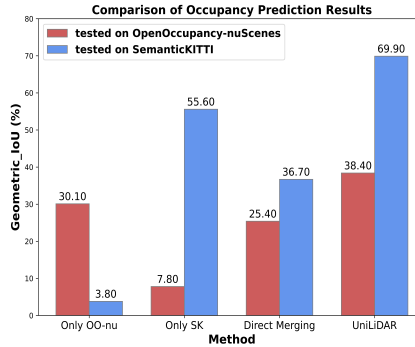


**Fig. 1:** Challenges in deploying a dataset-specific model to other datasets: 1) Only OO-nu and Only SK refer to the baseline model trained on each individual dataset [2, 24]. 2) Direct Merging represents training the model on the simply merged dataset. 3) UniLiDAR denotes the proposed method trained on these two datasets.

platforms equipped with different LiDARs often results in notable performance degradation, as shown in Fig. 1, rendering it evident that this paradigm fails to yield a robust and generalizable perception model. This phenomenon primarily arises from substantial domain shifts. In terms of 3D data, the gaps among datasets are primarily manifest in two dimensions: 1) significant divergence in point cloud density stemming from variations in LiDAR beams and angular resolutions, as shown in Tab. 1, and 2), inconsistent semantic label spaces caused by disparate taxonomies.

Traditionally, addressing these challenges involves annotating data from the target domain followed by model fine-tuning. However, annotating a frame of LiDAR point cloud consumes approximately  $10\times$  more time-consuming than annotating an image [27]. Fully leveraging all available 3D data could mitigate the expenditure of time and resources. Furthermore, fine-tuning the model with a new dataset always leads to "**catastrophic forgetting**" [16], wherein the model discards previously acquired knowledge. A question naturally arises: can these limitations be alleviated by bridging the gap among different LiDARs and facilitating continual learning from all available diverse data sources?

**Table 1:** Differences of typical 3D LiDAR dataset for autonomous driving. HAR denotes horizontal angular resolution, VFOV denotes vertical field of view, and L, W, and H represent the length, width, and height of LiDAR range, respectively. GT shape denotes the ground truth of occupancy grids' shape.

Datasets	Beam	HAR	VFOV	Point Range	Collection Location	GT shape
SemanticKITTI [2]	64	0.08°	[−23.6°, 3.2°]	L=[−72.0, 72.0]m W=[−72.0, 72.0]m H=[−3.4, 3.0]m	Germany	[256, 256, 32]
OpenOccupancy-nuScenes [24]	32	0.08° – 0.33°	[−30.0°, 10.0°]	L=[−51.2, 51.2]m W=[−51.2, 51.2]m H=[−5.0, 3.0]m	USA/Singapore	[512, 512, 40]

Motivated by the aforementioned challenges, this paper presents UniLiDAR, a pioneering 3D occupancy prediction framework designed to bridge the domain gap among different LiDARs. Different from predominant LiDAR-based perception algorithms [13, 17, 33, 34] that focus on devising an effective framework validated on a singular dataset, UniLiDAR endeavors to furnish a methodology

to facilitate existing 3D perception models to learn from all available diversified 3D datasets, enhancing their performance when directly deployed to real-world scenarios and reducing time and cost during migration across LiDARs. UniLiDAR features a geometric realignment module to encapsulate unique statistical characteristics of each LiDAR dataset within our model, alongside a semantic label mapping to harmonize the label space across disparate datasets. These components empower the model to continually learn from diverse data, thus reinforcing its adaptability and performance across heterogeneous data domains.

To evaluate the efficacy of the proposed framework in bridging substantial domain gaps, we conduct comprehensive experiments on two prominent public 3D occupancy prediction datasets, i.e. OpenOccupancy-nuScenes [24] and SemanticKITTI [2]. The experimental results underscore the robust dataset-level generalization capability of our approach, enabling the model to learn continually from all available data and seamlessly adapt. UniLiDAR demonstrates remarkable performance on both datasets. It significantly surpasses the baseline trained on a singular dataset and outperforms the multi-modality SOTA methods, showcasing the superiority of the MDT paradigm.

## 2 Related Works

### 2.1 LiDAR-based Perception Algorithm

LiDAR-based models have taken center stage in various crucial perception tasks for autonomous vehicles, including **3D object detection**, **semantic segmentation**, and **scene completion**. In the pursuit of highly intelligent automated vehicles, traditional bounding boxes provided by object detection [10, 19, 23] fall short of representing the surrounding environment comprehensively. Semantic segmentation [13, 17, 33] aims to assign a category label to each individual point, transforming the perception task from sparse prediction to dense prediction paradigm, thus offering a more fine-grained description of the environment. However, a frame of LiDAR point cloud merely offers a geometric sample of the 3D world, resulting in inherent information gaps. This partial semantic representation struggles to describe obstacles with arbitrary shapes.

Semantic scene completion (SSC) [9, 26, 28], also known as semantic occupancy prediction [34], addresses the task of reconstructing the 3D environment from an incomplete and sparse observation, both at geometric and semantic. Diverging from discriminative tasks such as object detection and semantic segmentation, the output of this generative task is fine-grained semantic occupancy grids, presenting greater challenges but offering enhanced compatibility with downstream tasks. This characteristic motivates this paper to focus on the 3D semantic occupancy prediction task on two prominent datasets: OpenOccupancy-nuScenes of 32 beams LiDAR [24] and SemanticKITTI [2] of 64 beams LiDAR.

### 2.2 3D Occupancy Prediction

Vision-centric methods for occupancy prediction have gained prominence [14, 24, 25]. Wang et al. [24] introduced the pioneering benchmark **OpenOccupancy-**

**nuScenes** for surrounding semantic occupancy perception in driving scenarios. Meanwhile, SurroundOcc [25] proposed a pipeline for converting LiDAR points into arbitrary-resolution occupancy grids by poisson reconstruction, facilitating the supervision of multi-camera 3D occupancy prediction tasks. TPVFormer [14] introduced a novel tri-perspective view representation (TPV), which deviates from traditional voxel-based approaches, utilizing three orthogonal 2D planes to effectively model the 3D scene. However, it is noteworthy that LiDAR point clouds inherently contain richer and more accurate geometric information compared to images, LiDAR-based methods deserve more exploration.

Some early research [9, 26, 28] conducted on **SemanticKITTI** [2] explored the feasibility of LiDAR-based semantic scene completion and demonstrated commendable performance. PointOcc [34] transforms point clouds into TPV space and models fine-grained 3D structures through an efficient 2D image backbone, achieving comparable performance to voxel-based methods on OpenOccupancy-nuScenes. Nevertheless, all the aforementioned works follow a single dataset-specific training and testing paradigm. Consequently, these models are susceptible to significant performance degradation in deployment across LiDARs.

### 2.3 Multiple Datasets Training (MDT)

Training on multiple datasets is an effective strategy to enhance model robustness on vision-centric models [5, 18, 32]. Given the similar grid structure of images, the primary challenge in vision fields lies in unifying label space to ensure consistency in semantic output. Early approaches attempted manually crafting the taxonomy [1, 18], which are both labor-intensive and error-prone. With the development of large language models (LLM), differing from previous works on MDT paradigms, BigDetection [5] harnessed the power of BERT [11] to construct an initial unified label space across datasets and employed manual verification to obtain the final taxonomy. However, the aforementioned methods all necessitate extensive human annotation efforts, rendering them non-scalable to a larger scope. To solve this problem, Zhou et al. [32] introduced a fully automatic approach based on combinatorial optimization to unify the output space of a multi-dataset detection system by leveraging intrinsic data properties and achieving a common taxonomy based on similarity.

Unlike the consistency observed in images within the vision domain, 3D LiDAR datasets exhibit substantial disparities at both the geometric and semantic levels. Nevertheless, research on 3D multiple datasets training remains limited. Uni3D [31] stood out as the pioneering effort focused on 3D multi-dataset object detection. However, object detection is a sparse-prediction task, and Uni3D concentrates solely on three categories: vehicles, pedestrians, and cyclists. While it is a prevalent setting [29, 30], such an approach could potentially impede the models' generalization to real-world scenarios.

To the best of our knowledge, our UniLiDAR is the first pipeline to explore the LiDAR-based dense-predict task across multiple datasets.

### 3 Method

#### 3.1 Preliminary

**Problem Setting** In the context of semantic occupancy prediction from a single dataset, the task involves processing an input frame of LiDAR points  $\hat{X}_i \in \mathbb{R}^{N \times 3}$  to predict the corresponding occupancy labels  $\mathcal{F}(\hat{X}_i) \in \mathbb{R}^{H \times W \times Z}$ , where  $H$ ,  $W$ , and  $Z$  represent the volumetric dimensions of the entire scene.

Training an occupancy prediction model on a single dataset usually follows a simple recipe: minimize a total loss  $\ell$ , which often includes elements such as cross-entropy loss, semantic mIoU, and geometric IoU, across a set of sampled point clouds  $\hat{X}$  and its corresponding annotated occupancy ground truth  $\hat{L}$  from the dataset  $\mathcal{D}_i$ :

$$\min_{\Theta} \mathbb{E}_{(\hat{X}, \hat{L}) \in \mathcal{D}_i} \left[ \ell(\mathcal{F}(\hat{X}; \Theta), \hat{L}) \right]. \quad (1)$$

**Multiple Datasets Training** Consider a dataset characterized by a joint probability distribution  $P_{XL}$  over the input point cloud and label space  $\mathcal{X} \times \mathcal{L}$ . In multiple datasets training (MDT), we denote the number of datasets  $\mathcal{D}_i = (\mathbf{x}^{(i)}, \mathbf{l}^{(i)})_{i=1}^N$  by  $N$ , where each  $\mathcal{D}_i$  is associated with a unique data distribution  $P_{XL}^i$ . The objective of MDT is to leverage multiple labeled datasets  $\mathcal{D}$  to train a unified model that achieves a more generalizable function  $F: \mathcal{X} \rightarrow \mathcal{L}$ .

For MDT, a straightforward strategy is to merge all data into a significantly larger dataset  $\mathcal{D}_{total} = \mathcal{D}_1 \cup \mathcal{D}_2 \cup \dots$  and amalgamate their label spaces  $\mathcal{L}_{total} = \mathcal{L}_1 \cup \mathcal{L}_2 \cup \dots$ . This approach optimizes the same loss function over an expanded dataset:

$$\min_{\Theta} \mathbb{E}_{(\hat{X}, \hat{L}) \in \mathcal{D}_1 \cup \mathcal{D}_2 \cup \dots} \left[ \ell(\mathcal{F}(\hat{X}; \Theta), \hat{L}) \right] \quad (2)$$

Nonetheless, it is acknowledged that large-scale datasets exhibit naturally imbalanced class distributions [21]. In other words, a uniform loss function may not be applicable across all datasets. Consequently, training a model  $\mathcal{F}_k$  on a specific dataset  $\mathcal{D}_k$  necessitates a dataset-specific loss function  $\ell_k$ :

$$\min_{\Theta} \mathbb{E}_{(\hat{X}, \hat{L}) \in \mathcal{D}_K} \left[ \ell_k(\mathcal{F}_k(\hat{X}; \Theta), \hat{L}) \right] \quad (3)$$

In the next section, we present the design of the UniLiDAR framework and show how to train a 3D perception model that performs well on all datasets.

#### 3.2 Overview of UniLiDAR

**Overview Framework** The ambition of UniLiDAR is to construct a comprehensive model capable of continually learning across  $K$  distinct datasets  $\mathcal{D}_1, \dots, \mathcal{D}_K$  with respective label spaces  $\mathcal{L}_1, \dots, \mathcal{L}_K$ , and dataset-specific loss functions  $\ell_1, \dots, \ell_K$ . Given the uniform task objective and similar data structure of the input, despite data shifts across different datasets, the network can share the backbone parameters and just use dataset-specific heads. This can be considered training  $K$  partitioned dataset-specific models  $\mathcal{F}_1, \dots, \mathcal{F}_K$  in parallel, where each dataset uses its own classification layer and loss at the end.

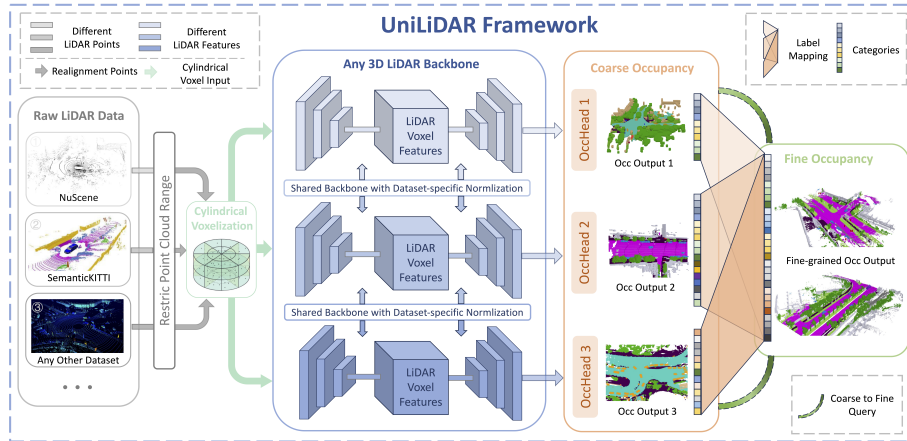


**Fig. 2:** The framework of UniLiDAR including: 1) point range alignment, 2) cylindrical voxelization, 3) shared 3D backbone with dataset-specific normalization, 4) dataset-specific occupancy heads, 5) semantic label mapping, and 6) coarse to fine stage.

The objective of the training process is to minimize the cumulative loss across all datasets, as formalized in the following equation:

$$\min_{\Theta} \mathbb{E}_{D_k} \left[ \mathbb{E}_{(\hat{X}, \hat{L}) \in D_k} \left[ \ell_k(\mathcal{F}_k(\hat{X}; \Theta), \hat{L}) \right] \right] \quad (4)$$

The UniLiDAR framework is comprehensively illustrated in Fig. 2, showcasing the sequential processing stages from the intake of raw LiDAR data to the generation of fine-grained occupancy outputs. When evaluated in-domain, due to the knowledge is pre-acquired, only corresponding head yields predictions. When evaluated out-of-domain, all heads yield predictions to enhance robustness.

The core components of UniLiDAR include a geometric realignment module and a semantic label mapping module. The former involves point range alignment and dataset-specific normalization to ensure adaptability across different LiDARs. The latter is conducted on the output to convert the original categories to a unified label space. Inspired by OpenOccupancy [24], UniLiDAR incorporates an upsampling process for coarse-grained occupancy grids through geometric coarse-to-fine queries. While the primary objective of upsampling is to balance model performance with GPU memory usage, we posit that it serves to achieve self-regression outputs through a non-autoregressive mode, thereby enhancing the model’s efficiency and effectiveness.

Subsequent sections will detail the core components of UniLiDAR, delve into the mechanism of geometric realignment for bridging the domain gap among different LiDARs (Sec. 3.3), and outline the process of label space unification through label mapping based on combinatorial optimization (Sec. 3.4).

### 3.3 Geometric Realignment

**Geometric Disparities** Unlike 2D images, which are organized into a fixed grid structure of pixels, 3D point clouds are acquired through a set of lasers that varies

across LiDARs, so inherently unordered. This variability introduces a geometric distributional discrepancy across datasets. The principal differences between the two datasets under study are detailed in Tab. 1. Drawing inspiration from Uni3D [31], we investigate the impact of point cloud range on dense-predictive generative tasks. The results, delineated in Tab. 2, prompt us to implement distinctly different restriction strategies based on the task at hand.

For the object detection task, Uni3D [31] advocates for the utilization of the maximum point cloud range as a metric for correction. This approach is justified by the observation that objects are typically located within areas covered by the LiDAR point cloud returns. Consequently, selecting an extended range enhances the model’s capability to detect objects at greater distances. However, our analysis, as summarized in Tab. 2, reveals that employing the maximum point cloud range for realignment in dense-predict generative tasks adversely affects performance. The discrepancy in occupancy grid shapes and annotation ranges can disrupt the learning process, leading to confusion in areas of annotation inconsistency. Therefore, opting for the minimum point cloud range for the occupancy prediction task yields more favorable outcomes than the maximum.

**Table 2:** Inconsistent LiDAR ranges will cause a significant model performance drop. For the intuitiveness of presentation, we only show the geometric IoU. The model employs L-CONet [24] trained on both datasets.

Methods	OpenOccupancy-nuScenes Range	SemantickittiKITTI Range	tested on OO-nu geometric IoU	tested on SK geometric IoU
Not Align.	L=[-51.2, 51.2]m W=[-51.2, 51.2]m H=[-5.0, 3.0]m	L=[-72.0, 72.0]m W=[-72.0, 72.0]m H=[-3.4, 3.0]m	25.4	36.7
Align Max	L=[-51.2, 51.2]m W=[-51.2, 51.2]m H=[-5.0, 3.0]m	L=[-51.2, 51.2]m W=[-51.2, 51.2]m H=[-5.0, 3.0]m	16.5(-8.9)	53.1(+16.4)
Align Min(UniLiDAR)	L=[0, 51.2]m W=[-25.6, 25.6]m H=[-3.4, 3.0]m	L=[0, 51.2]m W=[-25.6, 25.6]m H=[-3.4, 3.0]m	<b>38.4(+13.0)</b>	<b>69.9(+33.2)</b>

**Geometric Statistic Data Alignment** Inspired by prior studies [7, 31], a geometric statistic data realignment operation is introduced to bridge the domain gap among different LiDAR points. Our objective is to encapsulate the unique statistical characteristics of each LiDAR dataset within our model framework. The dataset-specific normalization strategy is delineated as Eq. (5):

$$\hat{y}_k^j = \gamma^j \hat{x}_k^j + \beta^j = \gamma^j \frac{x_k^j - \mu_k^j}{\sqrt{\sigma_k^j + \xi}} + \beta^j \quad (5)$$

where the  $\mu_k^j$  and  $\sigma_k^j$  represent the dataset-specific mean and variance corresponding to the input samples, the  $\xi$  is introduced for numerical stability, and the transformation parameters  $\gamma$  and  $\beta$  are utilized to restore the model’s representational capacity.

Traditional BatchNorm [15] estimates the statistical properties of the data within the current batch by standardizing the inputs for each layer across a network to attain a mean  $\mu^j$  of zero and a standard deviation  $\sigma^j$  of one. However, this conventional normalization relying on shared statistics does not make sense

and may impact model performance in MDT, where data within one batch may originate from different datasets. Therefore, we utilize dataset-specific mean and variance to encapsulate diverse statistical data. Notably,  $\gamma$  and  $\beta$  are shared across datasets. This strategy is justified by the alignment of inter-dataset discrepancies in first and second-order statistics post-normalization, thereby rationalizing the adoption of uniform  $\gamma$  and  $\beta$  parameters across diverse datasets.

This technique can be seamlessly integrated with previous 3D perception models, enhancing their adaptability and performance across diverse data sources.

### 3.4 Semantic Label Mapping

**Semantic Level Differences** The discrepancies in class definitions and annotation granularities among different datasets pose a significant challenge in MDT. For instance, SemanticKITTI [2] distinguishes static and dynamic objects (e.g., 'car' vs. 'moving-car'), which is crucial for scene understanding. Furthermore, it aggregates certain object categories into broader classes (e.g., 'other-vehicle' encompasses buses and rail vehicles) and delineates categories for road infrastructure ('road', 'parking', 'sidewalk') and natural elements ('vegetation', 'terrain'). Conversely, nuScenes [4] focuses on distinguishing various vehicle types (e.g., 'car', 'truck', 'bus') and explicitly categorizes urban infrastructure elements such as 'traffic-cone'. It also clearly segregates 'driveable surface' from 'sidewalk', establishing a distinct boundary between zones that are navigable by vehicles and those meant for pedestrian use.

Besides, the distribution of point clouds varies significantly across datasets, owing to their collection from diverse geographical locales via different LiDARs, as depicted in Tab. 1. Such heterogeneity engenders pronounced disparities in road topographies and object dimensions, as exemplified by the visualizations presented in Fig. 4.

**Learn a Unified Label Space** In the realm of MDT, each dataset with its own label space  $\mathcal{L}_1, \mathcal{L}_2, \dots$ , collectively ascertain a unified label space  $\mathcal{L}$ . This involves establishing a mapping function  $\mathcal{T}_k : \mathcal{L} \rightarrow \mathcal{L}_k$  for each dataset, enabling the conversion of dataset-specific labels to a unified label space. Furthermore, the transformation  $\mathcal{T}_j \mathcal{T}_i^\top$  facilitates the translation of output categories from label space  $\mathcal{L}_i$  to another  $\mathcal{L}_j$ .

Previous studies [29–31] predominantly adopted a straightforward approach for label space merging, i.e. select the important intersection of label spaces, other labels are removed, as illustrated in Fig. 3a. This methodology limits their focus to a narrow subset of categories—namely, vehicles, pedestrians, and cyclists—due to their importance in the domain of autonomous driving. While this is a common setting, such an approach could impede the models' generalization to real-world scenarios. To address this limitation, we introduce a novel method for automatically deriving a label space union encompassing a broader spectrum of categories from various datasets, as depicted in Fig. 3b. This strategy enhances the model's generalization ability by incorporating a more extensive and



representative set of categories, aligning more closely with real-world environments' complex and varied nature. By incorporating this expanded label space, we expect the model to generalize to the "open-set" real world ultimately.

Mathematically,  $\mathcal{T}_k \in \{0, 1\}^{|\mathcal{L}_k| \times |\mathcal{L}|}$  represents a boolean linear transformation. Each label specific to a dataset, denoted as  $l_k \in \mathcal{L}_k$ , is associated with precisely one unified label  $l_{\text{uni}} \in \mathcal{L}$ :  $\mathcal{T}_k \mathbf{1} = \mathbf{1}$ . Furthermore, each unified label corresponds to at most one dataset-specific label:  $\mathcal{T}_k^\top \mathbf{1} \leq \mathbf{1}$ . This implies that no dataset contains duplicate classes. This approach does not establish hierarchical relationships across datasets. It maintains all granularities within the unified label space in cases of varying label granularities.

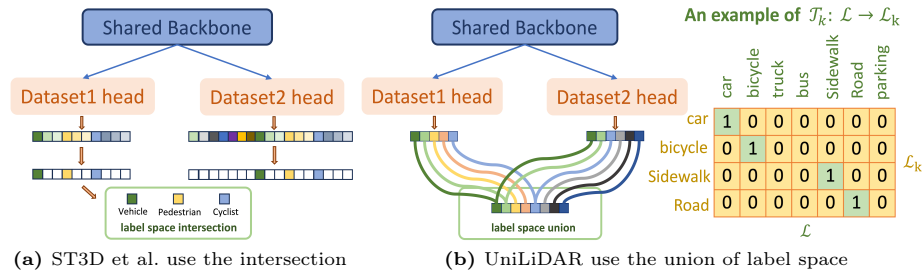


**Fig. 3:** Comparison of previous label space intersection and our unified label space

Given a set of dataset-specific models' outputs  $o_i^1 \in \mathbb{R}^{|\mathcal{L}_1|}$ ,  $o_i^2 \in \mathbb{R}^{|\mathcal{L}_2|}$ , ..., we construct a joint prediction score  $d_i$  by averaging the outputs of common classes:

$$d_i = \frac{\sum_k \mathcal{T}_k^\top o_i^k}{\sum_k \mathcal{T}_k^\top \mathbf{1}}, \quad (6)$$

where the division is elementwise. The dataset-specific outputs can be restored by  $\hat{o}_i^k = \mathcal{T}_k d_i$ . Our goal is to find a set of mappings  $\mathcal{T} = [\mathcal{T}_1 \dots, \mathcal{T}_N]$  and implicitly define a unified label-space  $\mathcal{L}$  such that the performance of the joint classifier remains unaffected. In other words, we seek to optimize the label mapping function by maximizing the similarity among the results obtained through two reciprocal mappings  $\mathcal{T}_k \mathcal{T}_k^\top o_i^k$ : from a specific dataset to a learned unified label space and back to the specific dataset label space.

Simple baselines encompass manually crafted mappings  $\mathcal{T}$  and label spaces  $\mathcal{L}$  [1, 18], or language-based merging [5]. Nevertheless, these methodologies encounter the hurdle of label ambiguity, necessitating significant human intervention for label rectification. In contrast, inspired by Zhou et al. [32], we introduce a data-driven optimization method that leverages correlations within the output of pre-trained occupancy prediction models across diverse LiDAR datasets, acting as a surrogate for perceptual similarity.

Further analysis of  $\mathcal{T}_k$  facilitates subsequent efficient optimization. First, note that the cardinality of label set  $\mathcal{L}$  corresponds to the number of columns in  $\mathcal{T}$ . Additionally, we merge at most one label per dataset, i.e.,  $\mathcal{T}_k^\top \mathbf{1} \leq \mathbf{1}$ . Thus, for each dataset  $\mathcal{D}_k$  a column  $\mathcal{T}_k(c) \in \mathbb{T}_k$  takes on one of  $|\mathcal{L}_k| + 1$  values:  $\mathbb{T}_k = \{\mathbf{0}, \mathbf{1}_1, \mathbf{1}_2, \dots\}$ , where  $\mathbf{1}_i \in \{0, 1\}^{|\mathcal{L}_k|}$  serves as an indicator vector of the  $i$ -th

element. Each column  $\mathcal{T}(c) \in \mathbb{T}$  selects from a limited set of potential values  $\mathbb{T} = \mathbb{T}_1 \times \mathbb{T}_2 \times \dots$ , with  $\times$  representing the Cartesian product. Instead of optimizing directly over the label set  $\mathcal{L}$  and transformation  $\mathcal{T}$ , we adopt combinatorial optimization over the potential column values of  $\mathbf{t} \in \mathbb{T}$ . Let  $x_{\mathbf{t}} \in \{0, 1\}$  denote whether combination  $\mathbf{t} \in \mathbb{T}$  is selected. In this formulation, the constraint  $\mathcal{T}_k \mathbf{1} = \mathbf{1}, \forall k \in N$  translates to  $\sum_{\mathbf{t} \in \mathbb{T} | t(c)=1} x_{\mathbf{t}} = 1$  for all dataset-specific labels  $c$ .

For a specific output class  $c$ , let  $\ell_c$  signify a loss function that assesses the fidelity of the unified label space  $l_{\text{uni}} \in \mathcal{L}$  and its re-projections  $\hat{l}_i^k$  concerning to the original disjoint label-space  $l_i^k \in \mathcal{L}_k$  on the occupancy grids  $i$ . Consider  $O^k = [o_1^k, o_2^k, \dots]$  as the outputs of the dataset-specific occupancy head for dataset  $\mathcal{D}_k$ . We define  $D = \frac{\sum_k \mathcal{T}_k^\top O^k}{\sum_k \mathcal{T}_k^\top \mathbf{1}}$  as the merged occupancy prediction scores, and  $\tilde{O}^k = \mathcal{T}_k D$  as the re-projection. Building upon our earlier analysis of the nature of  $\mathcal{T}_k$ , our objective is to minimize this loss across all dataset-specific outputs while respecting the boolean constraints imposed on our mapping:

$$\mathcal{J} = \sum_{\mathbf{t} \in \mathbb{T}} x_{\mathbf{t}} E_{\mathcal{D}_k} \underbrace{\left[ \sum_{c \in \mathcal{L}_k | t(c)=1} \mathcal{L}_c(O_c^k, \tilde{O}_c^k) \right]}_{c_{\mathbf{t}}} + \lambda \sum_{\mathbf{t} \in \mathbb{T}} x_{\mathbf{t}}. \quad (7)$$

Here, the penalty term  $\lambda \sum_{\mathbf{t} \in \mathbb{T}} x_{\mathbf{t}}$  is introduced to promote a small and concise label space. The merge cost  $c_{\mathbf{t}}$  can be precomputed for any subset of labels  $\mathbf{t}$  facilitating a computationally efficient approach. This yields a concise integer linear programming formulation of the objective Eq. (7):

$$\begin{aligned} & \text{minimize}_x && \mathcal{J} = \sum_{\mathbf{t} \in \mathbb{T}} x_{\mathbf{t}} (c_{\mathbf{t}} + \lambda) \\ & \text{subject to} && \sum_{\mathbf{t} \in \mathbb{T} | t(c)=1} x_{\mathbf{t}} = 1 \quad \forall c \in \mathcal{L}_k \end{aligned} \quad (8)$$

For the scenario involving two datasets, this objective equals to weighted bipartite matching. For a higher number of datasets, it reduces to weighted graph matching and is NP-hard yet practically solvable with integer linear programming. One drawback of this combinatorial reformulation is the exponential growth of the set of potential combinations  $\mathbb{T}$  with the number of datasets employed:  $|\mathbb{T}| = O(|\hat{\mathcal{L}}_1| |\hat{\mathcal{L}}_2| |\hat{\mathcal{L}}_3| \dots)$ . A one-by-one paradigm can be utilized to progressively unify additional datasets to address this challenge.

## 4 Experiments

### 4.1 Task Description and Benchmark

The 3D semantic occupancy prediction has garnered significant attention for autonomous driving, necessitating the assignment of semantic labels to all regions within the spatial domain. Our evaluation is conducted on two widely recognized datasets for autonomous driving occupancy prediction: SemanticKITTI [2] and

OpenOccupancy-nuScenes [24]. In SemanticKITTI, the dataset’s perceptive field spans the range from  $[-72.0m, -72.0m, -3.4m]$  to  $[72.0m, 72.0m, 3m]$ . However, the annotated region is restricted from  $[0m, -25.6m, -3.4m]$  to  $[51.2m, 25.6m, 3m]$ , featuring a voxel resolution of  $0.2m$ , thereby yielding in a volumetric representation of  $256 \times 256 \times 32$  voxels for occupancy prediction. Conversely, OpenOccupancy-nuScenes extends its perceptual range from  $[-51.2m, -51.2m, -5m]$  to  $[51.2m, 51.2m, 3m]$ , maintaining an identical voxel resolution of  $0.2m$ , resulting in a volumetric grid of  $512 \times 512 \times 40$  voxels for occupancy prediction. Our analysis is confined to the intersection of ground truth ranges, as delineated in Sec. 3.3, specifically from  $[0m, -25.6m, -3.4m]$  to  $[51.2m, 25.6m, 3m]$ . The evaluation employs the semantic metric **mIoU** and the geometric metric **IoU**, following the methodology outlined in OpenOccupancy [24].

## 4.2 Implementation Details

**Model Architecture.** Our methodology adopts the architectural framework utilized by L-baseline and L-CONet [24] across both datasets. The input points are configured to perform cylindrical partitioning with dimensions  $(\mathcal{H}_{in}, \mathcal{W}_{in}, \mathcal{D}_{in}) = (512, 360, 32)$ , representing radius, angle, and height, respectively. Within the encoder, we employ Resnet3D [12] as the 3D backbone, augmented by an FPN [20] to integrate features across multiple scales. The occupancy head produces a voxel representation of dimensions  $(\mathcal{H}_{out}, \mathcal{W}_{out}, \mathcal{D}_{out}) = (128, 90, 8)$ . To enhance performance, we adopt a coarse-to-fine query strategy to upsample the output by a factor of  $s = 4$ , following the methodology of L-CONet.

**Optimization.** During training on both datasets, we employ the Adam optimizer complemented by a weight decay of 0.01. A cosine learning rate scheduler initiates with a peak value of  $3e - 4$ , accompanied by a linear warm-up phase for the initial 500 iterations. The occupancy prediction leverages a combination of classic cross-entropy loss, Lovasz-softmax loss [3], and an affinity loss to concurrently optimize the geometry and semantic metrics [6].

**Detailed Setting.** All experimental procedures were executed using the mmdetection3d framework. Notably, disparities in point cloud range significantly impacted cross-dataset detection performance, as outlined in Tab. 2. To mitigate this issue, we standardized the point cloud ranges across all datasets to  $[0, 51.2]m$  along the  $X$  axis,  $[-25.6, 25.6]m$  along the  $Y$  axis, and  $[-3.4, 3]m$  along the  $Z$  axis, aligning with the intersecting range of the datasets under consideration. All models undergo training for 24 epochs, with a batch size of 8, distributed across 8 RTX 3090 GPUs. For the OpenOccupancy-nuScenes benchmark, we utilize multiple (10) LiDAR sweeps as input, adhering to a widely accepted practice. Conversely, for the SemanticKITTI dataset, a single LiDAR sweep is utilized as input.

Moreover, to ensure gradient backward propagation through all network parameters and sustain the training process, we design a balanced distributed group sampler that integrates data from distinct datasets in each batch. To the best of our knowledge, UniLiDAR pioneers the application of the scene completion task on mmdetection3d and explores the MDT paradigm within this framework.

### 4.3 3D Semantic Occupancy Prediction Results

As depicted in Tab. 3 and Tab. 4, our proposed UniLiDAR effectively bridges the domain gap among disparate LiDAR datasets, thereby facilitating continual learning from diverse data sources.

**Table 3: 3D Semantic occupancy prediction results on OpenOccupancy-nuScenes [24].** We report the performance on semantic scene completion (SSC - mIoU) and geometric scene completion (SC - IoU) for LiDAR-inferred baselines and our method. The C, L, and D denotes camera, LiDAR, and depth, respectively.

Method	Input	IoU	mIoU	barrier	bicycle	bus	car	const. veh.	motorcycle	pedestrian	traffic cone	trailer	truck	drive. surf.	other flat	sidewalk	terrain	manmade	vegetation
				■	■	■	■	■	■	■	■	■	■	■	■	■	■	■	■
MonoScene [6]	C	18.4	6.9	7.1	3.9	9.3	7.2	5.6	3.0	5.9	4.4	4.9	4.2	14.9	6.3	7.9	7.4	10.0	7.6
TPVFormer [14]	C	15.3	7.8	9.3	4.1	11.3	10.1	5.2	4.3	5.9	5.3	6.8	6.5	13.6	9.0	8.3	8.0	9.2	8.2
3DSketch [8]	C&D	25.6	10.7	12.0	5.1	10.7	12.4	6.5	4.0	5.0	6.3	8.0	7.2	21.8	14.8	13.0	11.8	12.0	21.2
LMSNet [22]	L	27.3	11.5	12.4	4.2	12.8	12.1	6.2	4.7	6.2	6.3	8.8	7.2	24.2	12.3	16.6	14.1	13.9	22.2
JS3C-Net [28]	L	30.2	12.5	14.2	3.4	13.6	12.0	7.2	4.3	7.3	6.8	9.2	9.1	27.9	15.3	14.9	16.2	14.0	24.9
C-CONet [24]	C	20.1	12.8	13.2	8.1	15.4	17.2	6.3	11.2	10.0	8.3	4.7	12.1	31.4	18.8	18.7	16.3	4.8	8.2
L-CONet [24]	L	30.9	15.8	17.5	5.2	13.3	18.1	7.8	5.4	9.6	5.6	13.2	13.6	34.9	21.5	22.4	21.7	19.2	23.5
M-CONet [24]	C&L	29.5	20.1	<b>23.3</b>	13.3	21.2	24.3	<b>15.3</b>	<b>15.9</b>	18.0	<b>13.3</b>	<b>15.3</b>	20.7	33.2	21.0	22.5	21.5	19.6	23.2
SurroundOcc [25]	C	31.5	20.3	20.6	11.7	<b>28.0</b>	<b>30.9</b>	10.7	15.1	14.1	12.1	14.4	<b>22.3</b>	<b>37.3</b>	<b>23.7</b>	24.5	22.8	14.9	21.9
PointOcc [34]	L	<b>34.1</b>	<b>23.9</b>	<b>24.9</b>	19.0	20.9	<b>25.7</b>	<b>13.4</b>	<b>25.6</b>	<b>30.6</b>	<b>17.9</b>	<b>16.7</b>	<b>21.2</b>	36.5	<b>25.6</b>	<b>25.7</b>	<b>24.9</b>	<b>24.8</b>	<b>29.0</b>
UniLiDAR (D.M.)(ours)	L	25.4	5.7	2.0	0.1	1.4	5.4	0.3	0.3	0.4	0.3	2.8	2.5	28.1	10.3	10.9	10.3	6.5	9.9
UniLiDAR (Tr.both)(ours)	L	<b>38.4</b>	<b>21.4</b>	<b>24.9</b>	<b>57.0</b>	<b>22.0</b>	<b>25.7</b>	11.7	15.4	<b>18.5</b>	<b>13.3</b>	13.9	19.7	<b>39.5</b>	15.9	<b>26.3</b>	<b>25.7</b>	<b>29.8</b>	<b>34.5</b>

The experimental results underscore the robust dataset-level generalization capabilities of UniLiDAR. Specifically, without bells and whistles, for the OpenOccupancy-nuScenes, UniLiDAR enhances occupancy prediction geometric **IoU** and semantic **mIoU** by **13.0%** and **15.7%** compared to training on the directly merged dataset, respectively. In the case of SemanticKITTI, UniLiDAR improves the occupancy prediction accuracy of **33.20%** and **12.50%** compared to training on the directly merged dataset, respectively, marking a significant advancement in performance.

**Table 4: 3D Semantic occupancy prediction results on SemanticKITTI [2].** We select the same metric as OpenOccupancy-nuScenes.

Method	Input	IoU	mIoU	road (13.30%)	sidewalk (11.13%)	pavement (1.12%)	other-grad (0.56%)	building (14.1%)	car (3.92%)	truck (0.16%)	bicycle (0.03%)	motorcycle (0.03%)	other-veh. (0.20%)	vegetation (39.3%)	trunk (0.41%)	terrain (0.17%)	pole (0.07%)	bicyclist (0.07%)	motorcycl. (0.03%)	fence (3.60%)	pole (0.20%)	traf.-sign (0.08%)
				■	■	■	■	■	■	■	■	■	■	■	■	■	■	■	■	■	■	■
LMSNet [22]	L	31.38	7.07	46.70	19.50	13.50	3.10	10.30	14.30	0.30	0.00	0.00	0.00	10.80	0.00	10.40	0.00	0.00	0.00	5.40	0.00	0.00
3DSketch [8]	C&D	26.85	6.23	37.70	19.80	0.00	0.00	12.10	17.10	0.00	0.00	0.00	0.00	12.10	0.00	16.10	0.00	0.00	0.00	3.40	0.00	0.00
JS3C-Net [28]	L	34.00	8.97	47.30	21.70	19.90	2.80	12.70	20.10	0.80	0.00	0.00	4.10	14.20	3.10	12.40	0.00	0.20	0.20	8.70	1.90	0.30
MonoScene [6]	C	34.16	11.08	54.70	27.10	24.80	5.70	14.40	18.80	3.30	0.50	0.70	<b>4.40</b>	14.90	2.40	<b>19.50</b>	1.00	1.40	0.40	11.10	3.30	2.10
SurroundOcc [25]	C	34.72	11.86	<b>56.90</b>	<b>28.30</b>	<b>30.20</b>	<b>6.80</b>	15.20	20.60	1.40	<b>1.60</b>	<b>1.20</b>	<b>4.40</b>	14.90	3.40	19.30	<b>1.40</b>	<b>2.00</b>	0.10	<b>11.30</b>	<b>3.90</b>	<b>2.40</b>
SCPnet [26]	L	<b>56.10</b>	<b>36.70</b>	<b>68.50</b>	<b>49.80</b>	<b>51.30</b>	<b>30.70</b>	<b>38.80</b>	<b>46.40</b>	<b>13.80</b>	<b>33.20</b>	<b>34.90</b>	<b>29.10</b>	<b>46.40</b>	<b>40.10</b>	<b>48.70</b>	<b>28.20</b>	<b>24.70</b>	34.90	<b>44.70</b>	<b>40.40</b>	<b>25.10</b>
L-CONet [24]	L	55.60	4.70	20.20	6.10	1.60	0.00	1.70	2.30	0.00	0.00	0.00	0.50	0.00	6.50	0.00	0.00	<b>49.20</b>	1.00	0.10	0.00	
UniLiDAR (D.M.)(ours)	L	36.70	2.00	1.60	1.10	0.00	0.00	0.10	0.30	0.00	0.00	0.00	0.00	1.70	0.00	0.90	0.00	0.00	31.5	0.20	0.00	0.00
UniLiDAR (Tr.both)(ours)	L	<b>69.90</b>	<b>14.30</b>	35.40	19.30	3.40	0.00	<b>21.80</b>	<b>32.90</b>	<b>9.50</b>	0.00	0.50	1.00	<b>27.30</b>	<b>7.90</b>	18.20	0.50	0.30	<b>63.70</b>	7.30	<b>19.40</b>	<b>6.20</b>

Furthermore, UniLiDAR significantly outperforms baseline methods trained on individual datasets and surpasses the SOTA methods leveraging all input modalities on OpenOccupancy-nuScene benchmarks. Compared to the baseline L-CONet [24], UniLiDAR yields notable enhancements of **7.5%** and **5.6%** in **IoU** and **mIoU**, respectively, on the OpenOccupancy-nuScenes dataset; along with enhancements of **14.30%** and **9.80%** on the SemanticKITTI dataset. Moreover, UniLiDAR surpasses LiDAR-based method PointOcc [34] by **4.3%** in geometric

IoU. Additionally, it demonstrates superior performance compared to the SOTA multi-modality model M-CONet by **8.9%** and **1.3%** in **IoU** and **mIoU**, respectively, underscoring its efficacy in extracting insights from diverse datasets.

The visual comparison of occupancy prediction results generated by the primary methods is illustrated in Fig. 4. Additional visualizations can be found in the appendix.

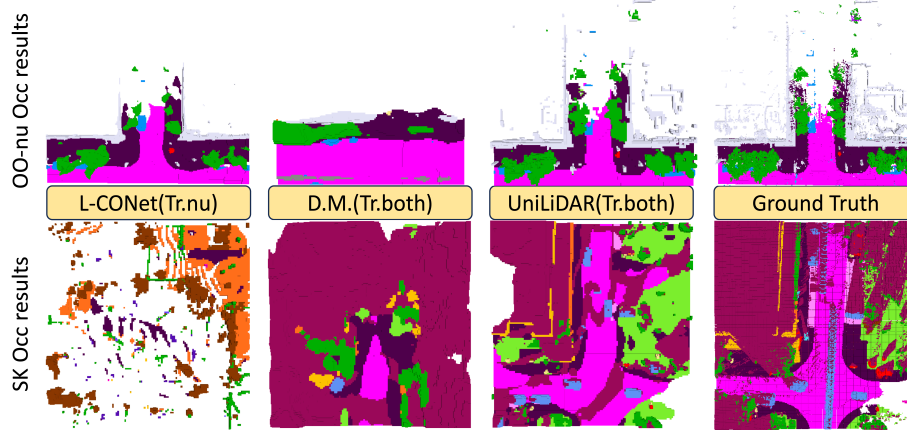


**Fig. 4:** Visualizations of occupancy prediction results. The upper half illustrates the outcomes of Openoccupancy-nuScene, while the lower half showcases the results obtained from SemanticKITTI.

#### 4.4 Ablution Experiments

**Design of Comparison Baselines** 1) **w/o P.T. (Single-dataset)**: We employ the off-the-shelf occupancy prediction network L-baseline and L-CONet [24], as the baseline occupancy prediction model, which is trained from scratch and evaluated within a single dataset.

2) **P.T. (Pre-training)**: We refer to the common fine-tune paradigm when dataset-specific models are deployed. The baseline model is first pre-trained on another dataset(source domain) and fine-tuned on the current dataset(target domain). The training process on the two datasets is independent.

3) **D.M. (Direct Merging)**: By simply combing multiple 3D datasets into a merged dataset, a dataset-specific model can be trained on it with a combined loss, which can be regarded as a direct method to verify whether the existing 3D models can be improved under the directly-merged datasets. Notably, we refrain from employing additional strategies to enhance performance for such a setting.

4) **G.R. (R.A.+G.A.)**: As introduced in Sec. 3.3, we conduct the point cloud range alignment(R.A.) and use the geometric statistical data alignment(G.A.) to bridge the domain gap among different LiDARs and encapsulate the unique statistical characteristics of each LiDAR dataset within our model framework.

**Further Analysis** 1) **Large disparity across 3D datasets**: As illustrated in Tab. 5, the dataset-specific models exhibit notable performance solely within

**Table 5:** Ablation results of core components of UniLiDAR on OpenOccupancy-nuScenes and SemanticKITTI datasets. SK denotes the SemanticKITTI dataset. OO-nu denotes the OpenOccupancy-nuScenes dataset.

Trained on	Method	Tested on OpenOccupancy-nuScenes		Tested on SemanticKITTI	
		Geometric IoU	Semantic mIoU	Geometric IoU	Semantic mIoU
only SK	UniLiDAR (w/o P.T.)	4.1	0.1	55.6	4.7
	UniLiDAR (w/ P.T. on OO-nu)	4.3(+0.2)	0.1	53.3(-2.3)	4.0(-0.7)
only OO-nu	UniLiDAR (w/o P.T.)	30.1	15.8	3.8	0.3
	UniLiDAR (w/ P.T. on SK)	26.3(-3.8)	7.1(-8.7)	5.7(+1.9)	0.1(-0.2)
SK+OO-nu	UniLiDAR (w/ D.M.)	25.4	5.7	36.7	2.0
	UniLiDAR (w/ G.A.)	14.7(-10.7)	1.6(-4.1)	51.2(+14.5)	3.0(+1.0)
	UniLiDAR (w/ R.A.)	38.2(+12.8)	21.3(+15.6)	70.0(+33.3)	13.4(+11.4)
	UniLiDAR (w/ G.R. (R.A.+G.A.))	38.4(+13.0)	21.4(+15.7)	69.9(+33.2)	14.5(+12.5)

their corresponding source domains. However, upon their application to other domains, their efficacy significantly diminishes. This phenomenon predominantly stems from the overfitting of dataset-specific models to their source domains, thereby overlooking the inherent shift from the source to the target dataset.

2) **Limited efficacy of pre-trained models and their detrimental impact on the target domain:** Adhering to the prevailing fine-tuning paradigm, we initially pre-train the baseline model on the source domain and subsequently fine-tune the model on the target domain. Upon comparing the baselines P.T and w/o P.T., as depicted in Tab. 5, it is evident that despite pre-training, instances of catastrophic forgetting persist, e.g. the model forgets knowledge acquired from the preceding pre-trained dataset. While there is a marginal enhancement within the source domain, the pre-existing knowledge impedes the models’ effectiveness within target domains.

3) **Assessment of Module Effectiveness and Generality:** By comparing w/ P.T. and D.M baselines from Tab. 5, it becomes evident that the 3D single-dataset training paradigm fails to yield a robust and generalizable perception model. As indicated in Tabs 3, 4, and 5, the geometric IoU and semantic mIoU attained by UniLiDAR surpass those of all baseline methods, thereby affirming the efficacy of UniLiDAR in bridging the domain gap across diverse datasets and learn continually from all available data.

Specifically, both R.A. and G.A. modules contribute to enhancing occupancy prediction accuracy. The minimum R.A. is deemed necessary under the dense-predict MDT setting, resulting in a significant improvement.

## 5 Conclusion

This paper pioneered the exploration of training strategies to construct a unified model capable of handling different LiDARs, enabling continual learning across diverse LiDAR datasets. The proposed UniLiDAR, which integrates geometric realignment and semantic label mapping, effectively tackled challenges stemming from dataset divergence, marking a notable advancement in 3D generalizable perception models, as validated by extensive experimentation on prominent benchmarks. While the proposed approach presently does not extend to handling unseen LiDARs, we will endeavor to resolve this limitation in the future.

## References

1. Object detection with a unified label space from multiple datasets | springerlink. [https://link.springer.com/chapter/10.1007/978-3-030-58568-6\\_11](https://link.springer.com/chapter/10.1007/978-3-030-58568-6_11) 4, 9
2. Behley, J., Garbade, M., Milioto, A., Quenzel, J., Behnke, S., Stachniss, C., Gall, J.: Semantickitti: A dataset for semantic scene understanding of lidar sequences. In: Proceedings of the IEEE/CVF International Conference on Computer Vision. pp. 9297–9307 (2019) 2, 3, 4, 8, 10, 12, 18, 20, 21
3. Berman, M., Triki, A.R., Blaschko, M.B.: The lovász-softmax loss: A tractable surrogate for the optimization of the intersection-over-union measure in neural networks. In: Proceedings of the IEEE Conference on Computer Vision and Pattern Recognition. pp. 4413–4421 (2018) 11
4. Caesar, H., Bankiti, V., Lang, A.H., Vora, S., Liong, V.E., Xu, Q., Krishnan, A., Pan, Y., Baldan, G., Beijbom, O.: Nuscenec: A multimodal dataset for autonomous driving. In: Proceedings of the IEEE/CVF Conference on Computer Vision and Pattern Recognition. pp. 11621–11631 (2020) 8, 20
5. Cai, L., Zhang, Z., Zhu, Y., Zhang, L., Li, M., Xue, X.: Bigdetection: A large-scale benchmark for improved object detector pre-training. In: Proceedings of the IEEE/CVF Conference on Computer Vision and Pattern Recognition. pp. 4777–4787 (2022) 4, 9
6. Cao, A.Q., de Charette, R.: Monoscene: Monocular 3d semantic scene completion. In: 2022 IEEE/CVF Conference on Computer Vision and Pattern Recognition (CVPR). pp. 3981–3991 (Jun 2022). <https://doi.org/10.1109/CVPR52688.2022.00396> 11, 12
7. Chattopadhyay, P., Sarangmath, K., Vijaykumar, V., Hoffman, J.: Proportional amplitude spectrum training augmentation for synthetic-to-real domain generalization (Sep 2022) 7
8. Chen, X., Lin, K.Y., Qian, C., Zeng, G., Li, H.: 3d sketch-aware semantic scene completion via semi-supervised structure prior. In: Proceedings of the IEEE/CVF Conference on Computer Vision and Pattern Recognition. pp. 4193–4202 (2020) 12
9. Cheng, R., Agia, C., Ren, Y., Li, X., Bingbing, L.: S3cnet: A sparse semantic scene completion network for lidar point clouds. In: Proceedings of the 2020 Conference on Robot Learning. pp. 2148–2161. PMLR (Oct 2021) 1, 3, 4
10. Deng, J., Shi, S., Li, P., Zhou, W., Zhang, Y., Li, H.: Voxel r-cnn: Towards high performance voxel-based 3d object detection. AAAI 35(2), 1201–1209 (May 2021). <https://doi.org/10.1609/aaai.v35i2.16207> 1, 3
11. Devlin, J., Chang, M.W., Lee, K., Toutanova, K.: Bert: Pre-training of deep bidirectional transformers for language understanding (May 2019). <https://doi.org/10.48550/arXiv.1810.04805> 4
12. He, K., Zhang, X., Ren, S., Sun, J.: Deep residual learning for image recognition. In: Proceedings of the IEEE Conference on Computer Vision and Pattern Recognition. pp. 770–778 (2016) 11
13. Hou, Y., Zhu, X., Ma, Y., Loy, C.C., Li, Y.: Point-to-voxel knowledge distillation for lidar semantic segmentation. In: Proceedings of the IEEE/CVF Conference on Computer Vision and Pattern Recognition. pp. 8479–8488 (2022) 1, 2, 3
14. Huang, Y., Zheng, W., Zhang, Y., Zhou, J., Lu, J.: Tri-perspective view for vision-based 3d semantic occupancy prediction. In: Proceedings of the IEEE/CVF Conference on Computer Vision and Pattern Recognition. pp. 9223–9232 (2023) 3, 4, 12

15. Ioffe, S., Szegedy, C.: Batch normalization: Accelerating deep network training by reducing internal covariate shift. In: Proceedings of the 32nd International Conference on Machine Learning. pp. 448–456. PMLR (Jun 2015) [7](#)
16. Kirkpatrick, J., Pascanu, R., Rabinowitz, N., Veness, J., Desjardins, G., Rusu, A.A., Milan, K., Quan, J., Ramalho, T., Grabska-Barwinska, A., Hassabis, D., Clopath, C., Kumaran, D., Hadsell, R.: Overcoming catastrophic forgetting in neural networks. Proceedings of the National Academy of Sciences **114**(13), 3521–3526 (Mar 2017). <https://doi.org/10.1073/pnas.1611835114> [2](#)
17. Lai, X., Chen, Y., Lu, F., Liu, J., Jia, J.: Spherical transformer for lidar-based 3d recognition (Mar 2023) [1, 2, 3](#)
18. Lambert, J., Liu, Z., Sener, O., Hays, J., Koltun, V.: Mseg: A composite dataset for multi-domain semantic segmentation. In: Proceedings of the IEEE/CVF Conference on Computer Vision and Pattern Recognition. pp. 2879–2888 (2020) [4, 9](#)
19. Lang, A., Vora, S., Caesar, H., Zhou, L., Yang, J., Beijbom, O.: PointPillars: Fast Encoders for Object Detection From Point Clouds (Jun 2019). <https://doi.org/10.1109/CVPR.2019.01298> [1, 3](#)
20. Lin, T.Y., Dollár, P., Girshick, R., He, K., Hariharan, B., Belongie, S.: Feature pyramid networks for object detection (Apr 2017). <https://doi.org/10.48550/arXiv.1612.03144> [11](#)
21. Oksuz, K., Cam, B.C., Kalkan, S., Akbas, E.: Imbalance problems in object detection: A review. IEEE Transactions on Pattern Analysis and Machine Intelligence **43**(10), 3388–3415 (Oct 2021). <https://doi.org/10.1109/TPAMI.2020.2981890> [5](#)
22. Roldão, L., de Charette, R., Verroust-Blondet, A.: Lmscnet: Lightweight multiscale 3d semantic completion. In: 2020 International Conference on 3D Vision (3DV). pp. 111–119 (Nov 2020). <https://doi.org/10.1109/3DV50981.2020.00021> [12](#)
23. Shi, S., Guo, C., Jiang, L., Wang, Z., Shi, J., Wang, X., Li, H.: Pv-rcnn: Point-voxel feature set abstraction for 3d object detection. In: Proceedings of the IEEE/CVF Conference on Computer Vision and Pattern Recognition. pp. 10529–10538 (2020) [1, 3](#)
24. Wang, X., Zhu, Z., Xu, W., Zhang, Y., Wei, Y., Chi, X., Ye, Y., Du, D., Lu, J., Wang, X.: Openoccupancy: A large scale benchmark for surrounding semantic occupancy perception (Mar 2023). <https://doi.org/10.48550/arXiv.2303.03991> [2, 3, 6, 7, 11, 12, 13, 18, 20, 21](#)
25. Wei, Y., Zhao, L., Zheng, W., Zhu, Z., Zhou, J., Lu, J.: Surroundocc: Multi-camera 3d occupancy prediction for autonomous driving (Mar 2023). <https://doi.org/10.48550/arXiv.2303.09551> [3, 4, 12, 20](#)
26. Xia, Z., Liu, Y., Li, X., Zhu, X., Ma, Y., Li, Y., Hou, Y., Qiao, Y.: Scpnet: Semantic scene completion on point cloud (Mar 2023). <https://doi.org/10.48550/arXiv.2303.06884> [1, 3, 4, 12, 20](#)
27. Xiao, A., Zhang, X., Shao, L., Lu, S.: A survey of label-efficient deep learning for 3d point clouds (May 2023) [2](#)
28. Yan, X., Gao, J., Li, J., Zhang, R., Li, Z., Huang, R., Cui, S.: Sparse single sweep lidar point cloud segmentation via learning contextual shape priors from scene completion. AAAI **35**(4), 3101–3109 (May 2021). <https://doi.org/10.1609/aaai.v35i4.16419> [1, 3, 4, 12](#)
29. Yang, J., Shi, S., Wang, Z., Li, H., Qi, X.: St3d: Self-training for unsupervised domain adaptation on 3d object detection. In: 2021 IEEE/CVF Conference on Computer Vision and Pattern Recognition (CVPR). pp. 10363–10373. IEEE, Nashville, TN, USA (Jun 2021). <https://doi.org/10.1109/CVPR46437.2021.01023> [4, 8](#)



30. Yang, J., Shi, S., Wang, Z., Li, H., Qi, X.: St3d++: Denoised self-training for unsupervised domain adaptation on 3d object detection. *IEEE Trans. Pattern Anal. Mach. Intell.* pp. 1–17 (2022). <https://doi.org/10.1109/TPAMI.2022.3216606> 4, 8
31. Zhang, B., Yuan, J., Shi, B., Chen, T., Li, Y., Qiao, Y.: Uni3d: A unified baseline for multi-dataset 3d object detection. In: *Proceedings of the IEEE/CVF Conference on Computer Vision and Pattern Recognition*. pp. 9253–9262 (2023) 4, 7, 8
32. Zhou, X., Koltun, V., Krähenbühl, P.: Simple multi-dataset detection. In: *Proceedings of the IEEE/CVF Conference on Computer Vision and Pattern Recognition*. pp. 7571–7580 (2022) 4, 9, 19
33. Zhu, X., Zhou, H., Wang, T., Hong, F., Ma, Y., Li, W., Li, H., Lin, D.: Cylindrical and asymmetrical 3d convolution networks for lidar segmentation. In: *Proceedings of the IEEE/CVF Conference on Computer Vision and Pattern Recognition*. pp. 9939–9948 (2021) 1, 2, 3
34. Zuo, S., Zheng, W., Huang, Y., Zhou, J., Lu, J.: Pointocc: Cylindrical tri-perspective view for point-based 3d semantic occupancy prediction (Aug 2023). <https://doi.org/10.48550/arXiv.2308.16896> 2, 3, 4, 12

## A Appendix

### A.1 Simplified Code

We provide a simplified version of the codebase for assessing the efficacy of UniLiDAR, which is accessible anonymously at [https://anonymous.4open.science/r/unilidar\\_simple-C817](https://anonymous.4open.science/r/unilidar_simple-C817).<sup>1</sup> By strictly adhering to the guidelines provided in the Readme.md file, users can train a unified occupancy prediction model showcasing outstanding performance on both the SemanticKITTI dataset [2] and the OpenOccupancy-nuScenes dataset [24].

A more comprehensive version of the codebase will be released in the near future.

### A.2 Coarse to Fine Stage

We use the geometric coarse to fine query to upsample the initial output, inspired by OpenOccupancy [24].

Specifically, the coarse occupancy  $O^{\mathcal{M}} \in \mathbb{R}^{\frac{D}{S} \times \frac{H}{S} \times \frac{W}{S} \times c}$  is first generated by the baseline model, where the occupied voxels  $V_o \in \mathbb{R}^{N_o \times 3}$  ( $N_o$  is the number of occupied voxels, and 3 denotes the  $(x, y, z)$  indices in voxel coordinates) are split as high-resolution occupancy queries  $Q_H \in \mathbb{R}^{N_o 8^{\eta-1} \times 3}$ :

$$Q_H = \mathcal{T}_{v \rightarrow w}(\mathcal{F}_s(V_o, \eta)), \quad (9)$$

where  $\mathcal{F}_s$  is the voxel split function (*i.e.*, for  $(x_0, y_0, z_0)$  in  $V_o$ , the split indices are  $\{x_0 + \frac{i}{\eta}, y_0 + \frac{j}{\eta}, z_0 + \frac{k}{\eta}\} (i, j, k \in (0, \eta - 1))$ ),  $\eta$  is the split ratio (typically set as 4), and  $\mathcal{T}_{v \rightarrow w}$  transforms the voxel coordinates to the world coordinates. Subsequently, we transform  $Q_H$  to voxel space to sample geometric features  $F^{\mathcal{G}} = \mathcal{G}_S(F^{\mathcal{F}}, \mathcal{T}_{w \rightarrow v}(Q_H))$  ( $\mathcal{G}_S$  is the *grid sample* function,  $\mathcal{T}_{w \rightarrow v}$  is the transformation from world coordinates to voxel coordinates). FC layers then regularize the sampled features to produce fine-grained occupancy predictions:

$$O^{\mathcal{G}} = \mathcal{G}_f(\mathcal{G}_f(F^{\mathcal{G}})), \quad (10)$$

where  $F^{\mathcal{G}}$  are FC layers. Finally,  $O^{\mathcal{G}}$  can be reshaped to the volumetric representation  $O^{\text{vol}} \in \mathbb{R}^{\frac{\eta D}{S} \times \frac{\eta H}{S} \times \frac{\eta W}{S} \times c}$ :

$$O^{\text{vol}}(x, y, z) = \begin{cases} O^{\mathcal{G}}(\mathcal{T}_{v \rightarrow q}(x, y, z)) & (x, y, z) \in \mathcal{T}_{w \rightarrow v}(Q_H) \\ \text{Empty Label} & (x, y, z) \notin \mathcal{T}_{w \rightarrow v}(Q_H), \end{cases} \quad (11)$$

where  $\mathcal{T}_{v \rightarrow q}$  transforms the voxel coordinates to indices of the high-resolution query  $Q_H$ . For LiDAR-based CONet that without multi-view 2D features, we only sample  $Q_H$  from  $F^{\mathcal{L}}$ .

<sup>1</sup> In case of encountering an error (e.g., a blank page) upon clicking this link, kindly refresh the webpage.

### A.3 Scope of Using Geometric Alignment

We investigate the optimal range for geometric statistical data alignment, referred to as the utilization range of the dataset-specific norm layer. We categorize the settings into two distinct configurations: (1) employing geometric alignment only at the backbone and (2) substituting all norm layers in the network with geometric alignment. The experimental results are delineated in Tab. 6, prompting us to advocate for using geometric alignment solely for the backbone in the network.

**Table 6:** Experimental results of different scopes of geometric alignment.

Trained on	Method	Tested on OpenOccupancy-nuScenes		Tested on SemanticKITTI	
		Geometric IoU	Semantic mIoU	Geometric IoU	Semantic mIoU
SK+OO-nu	UniLiDAR (G.A. for all)	37.0	21.2	68.7	14.2
	UniLiDAR (G.A. for backbone)	38.4(+1.4)	21.4(+0.2)	69.9(+1.2)	14.5(+0.3)

### A.4 More Illustration about Semantic Label Mapping

**Computation of Label Space Learning Algorithm** The size of our optimization problem scales linearly in the number of potential merges  $|\mathbb{T}|$ , which can grow exponentially in the number of datasets. To counteract this exponential growth, inspired by UniDet [32], we only consider sets of classes

$$\mathbb{T}' = \left\{ \mathbf{t} \in \mathbb{T} \mid \frac{c_{\mathbf{t}}}{|\mathbf{t}| - 1} \leq \tau \right\}.$$

For an aggressive enough threshold  $\tau$ , the number of potential merges  $|\mathcal{T}'|$  remains manageable. We greedily grow  $\mathcal{T}'$  by first enumerating all feasible two-class merges ( $|\mathbf{t}| = 2$ ), then three-class merges, and so on. The detailed algorithm diagram is shown in Algorithm 1. The time complexity of this greedy algorithm is  $O(|\mathcal{T}'| \max_i |\hat{L}^i|)$ .

**One by One Paradigm to Add New Datasets to the Unified Label Space** While the aspiration is to maintain large and comprehensive training domains and label spaces, practical scenarios often necessitate the inclusion of more fine-grained labels or specific testing domains. Upon establishing a unified label space from an existing set of training datasets, a straightforward label space expansion algorithm is employed to facilitate the addition of further datasets and labels after the unified model has been trained.

We adopt a one-by-one optimization paradigm. Specifically, we execute the unified model on the already merged dataset and train a domain-specific perception model on the new domain. Subsequently, the label space learning algorithm is applied to generate a new unified label space. This approach mitigates the computational overhead associated with merging more than two datasets.

---

**Algorithm 1:** Learning a unified label space

---

**Input** :  $\{\mathbf{o}_i, \hat{\mathbf{l}}_i\}_{i=1}^N$ : semantic occupancy grids ground truth and labels for each of the  $N$  training datasets  
 $\{\{\tilde{\mathbf{o}}_i^{(j)}, \tilde{\mathbf{l}}_i^{(j)}\}_{j=1}^N\}_{i=1}^N$ : predicted semantic occupancy grids with predicted classes in all datasets for each training dataset  
 $\lambda, \tau$ : hyper-parameters for algorithm

**Output**:  $L$ : unified label space  
 $\mathcal{T}$ : the transformation from each individual label space to the unified label space

- 1 // Compute potential merges and merge cost
- 2  $\hat{L} = \bigcup_i \hat{L}_i$  // Short-hand used to simplify notation
- 3  $\mathbb{T}_1 \leftarrow \{(l) | l \in \hat{L}\}$  // Set of single labels
- 4 Compute  $c_t$  for all single labels  $t \in \mathbb{T}$ . // 0 for most metrics
- 5 **for**  $n = 2 \dots N$  **do**
- 6      $\mathbb{T}_n \leftarrow \{\}$
- 7     **for**  $t \in \mathbb{T}_{n-1}$  **do**
- 8         **for**  $l \in \hat{L}$  **do**
- 9             **if**  $l$  and all labels in  $t$  are from different datasets **then**
- 10                 compute  $c_{t \cup \{l\}}$ .
- 11                 **if**  $\frac{c_{t \cup \{l\}}}{n-1} \leq \tau$  **then**
- 12                     Add  $t \cup \{l\}$  to  $\mathbb{T}_n$ .
- 13                 **end**
- 14             **end**
- 15         **end**
- 16     **end**
- 17 **end**
- 18  $\mathbb{T} \leftarrow \bigcup_{n=1}^N \mathbb{T}_n$
- 19 // Solve the ILP.
- 20  $\mathbf{x} \leftarrow \text{ILP\_solver}(c, \mathbb{T}, \lambda)$  // Solve equation (8).
- 21 Compute  $L, \mathcal{T}$  from  $\mathbf{x}$
- 22 **Return**:  $L, \mathcal{T}$

---

## A.5 Challenges of Merging Datasets

**Dataset Introduction.** Following the practice of popular scene completion models [24–26], our experiments are conducted on two prominent LiDAR semantic prediction benchmarks, namely, OpenOccupancy-nuScenes [4, 24] and SemanticKITTI [2].

SemanticKITTI comprises annotated outdoor LiDAR scans with 21 semantic labels, organized into 22 point cloud sequences. Sequences 00 to 10, 08, and 11 to 21 are designated for training, validation, and testing, respectively. From these, 19 classes are selected for training and evaluation after merging classes with distinct motion statuses and removing classes with sparse points.

As for OpenOccupancy-nuscene, it is a large-scale occupancy prediction dataset deriving from nuScenes. Since the 3D semantic and 3D detection labels are un-

available in the test set, Wang et al. [24] did not provide dense occupancy labels of the unseen test set. Consequently, we utilize the training set for model training and the validation set for evaluation purposes.

**The Metric of Occupancy Prediction** For 3D semantic occupancy prediction, we use the intersection over the union (IoU) of occupied voxels, ignoring their semantic class as the evaluation metric of the scene completion (SC) task and the mIoU of all semantic classes for the SSC task.

$$\begin{aligned} \text{IoU} &= \frac{TP}{TP + FP + FN} \\ \text{mIoU} &= \frac{1}{C} \sum_{i=1}^C \frac{TP_i}{TP_i + FP_i + FN_i} \end{aligned} \quad (12)$$

where  $TP$ ,  $FP$ ,  $FN$  indicate the number of true positive, false positive, and false negative predictions.  $C$  is the class number.

**Primary Aspiration and Challenges** In the quest for highly intelligent automated vehicles, scalability and generalizability emerge as pivotal characteristics in perception models. According to the scaling-law, data plays a crucial role in augmenting both performance and generalizability.

However, acquiring vehicle travel data poses significant challenges compared to other forms of visual or textual data. Particularly, obtaining 3D LiDAR data entails substantial expenses. Consequently, existing autonomous driving datasets exhibit limited data volumes, hindering the training of models with requisite scalability and generalization. The conventional single dataset training-and-testing paradigm confines the source data within a delimited domain. Fully exploiting all available 3D data holds promise for mitigating resource expenditure and enhancing performance.

Initially, we have made a lot of attempts to train a vanilla 3D perception model using multiple datasets by directly merging existing 3D datasets, such as merging OpenOccupancy-nuScenes [24] and SemanticKITTI [2]. However, we found that commonly employed 3D perception models failed to perform satisfactorily across both datasets, as shown in Fig. 1. This inadequacy stems from the substantial disparities inherent in 3D point clouds acquired by diverse LiDARs, as shown in Tab. 1, rendering previous 3D models incapable of effectively addressing the significant data shift.

Furthermore, in the architectural design of the models to accommodate diverse label spaces, the incorporation of multiple heads within the network is deemed imperative. To facilitate gradient backward propagation across all network parameters and sustain the training process, a balanced distributed group sampler has been designed. This sampler amalgamates data from disparate datasets within each batch, thereby ensuring that data for each batch is sequentially drawn from distinct datasets.

## A.6 Extended Visualization of Occupancy Prediction Results

Further visualization results of the proposed UniLiDAR are shown in Figs. 5 and 6.

For Fig. 5 and Fig. 6, we utilize the proposed UniLiDAR model trained jointly on OpenOccupancy-nuScenes and SemanticKITTI datasets and showcase the outcomes on the validation sets of these two datasets. These results comprehensively demonstrate our ability to achieve improved occupancy prediction simultaneously for OpenOccupancy-nuScenes and SemanticKITTI datasets using a single perception model.

Furthermore, owing to the denser ground truth annotations provided by the SemanticKITTI dataset, the outcomes yielded by UniLiDAR on the OpenOccupancy-nuScenes dataset manifest heightened credibility compared to the ground truth in certain areas, such as the drivable surface and the trunk, thereby underscoring the supremacy of MDT paradigm.

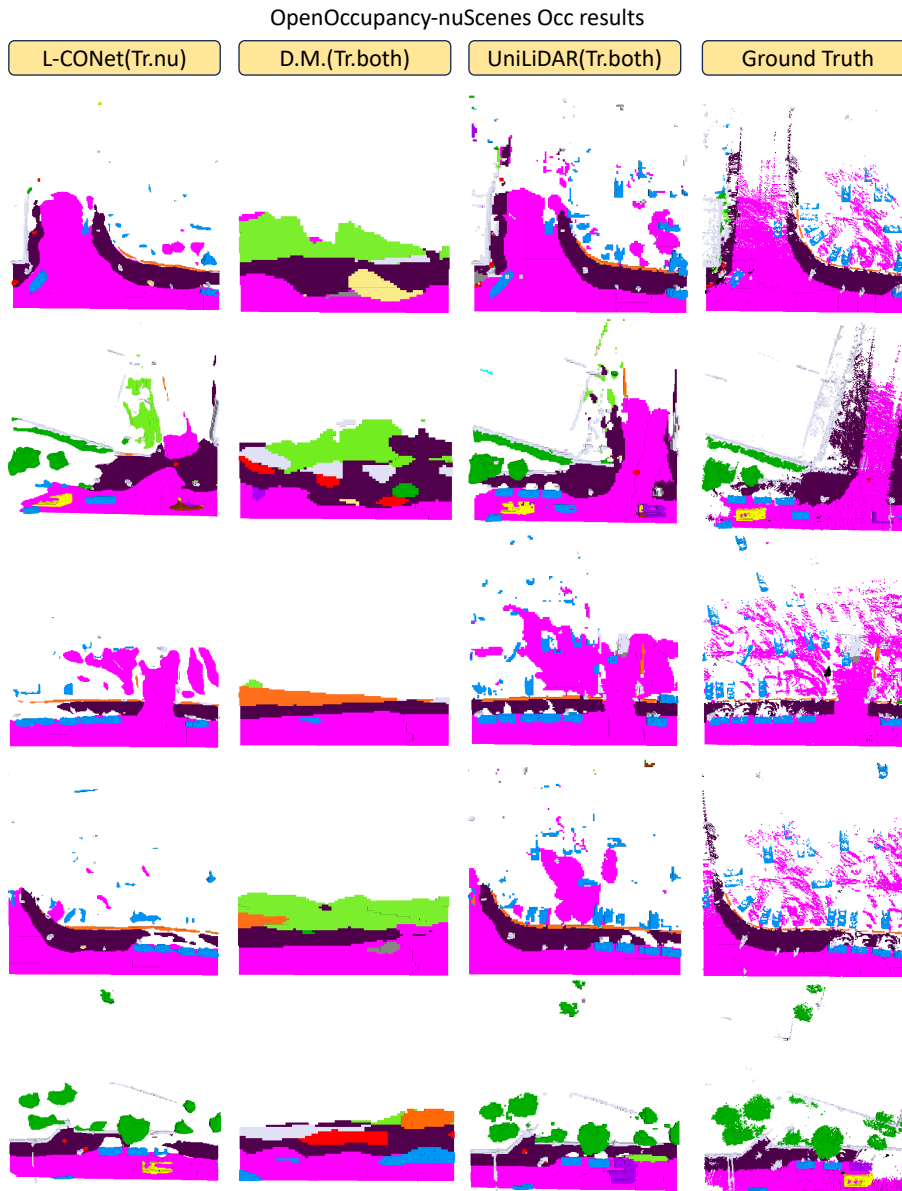


Fig. 5: Visualizations of occupancy prediction results on OpenOccupancy-nuScenes.

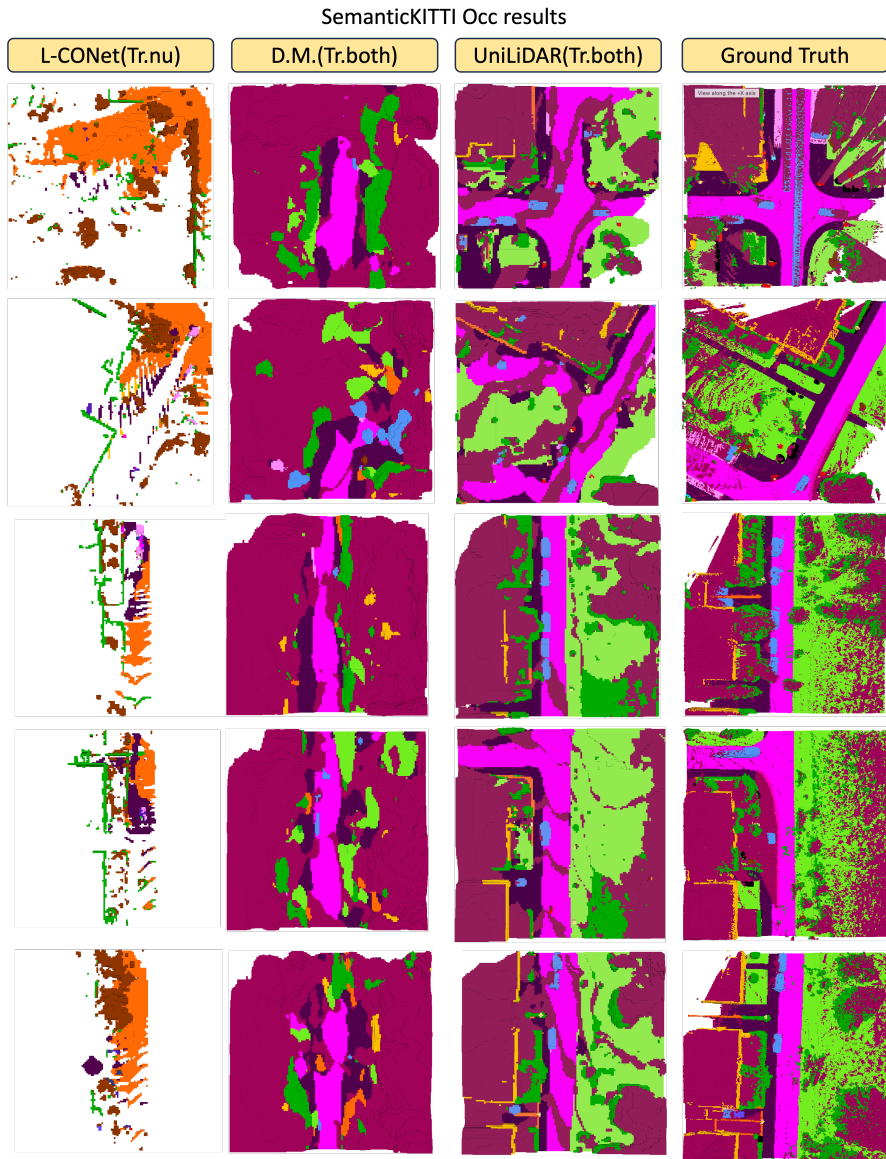


Fig. 6: Visualizations of occupancy prediction results on SemanticKITTI.